Supplementary Information

Exotic Long-Range Surface Reconstruction on $La_{0.7}Sr_{0.3}MnO_3$ Thin Films

Kyle P. Kelley[1], Vinit Sharma[2,3], Wenrui Zhang[4], Arthur P. Baddorf[1], Von B. Nascimento[5], Rama K. Vasudevan[1,*]

[1] Center for Nanophase Materials Sciences, Oak Ridge National Laboratory, Oak Ridge, TN 37831

[2] National Institute for Computational Sciences, Oak Ridge National Laboratory, Oak Ridge, TN 37831

[3] Joint Institute for Computational Sciences, University of Tennessee, Knoxville, TN, 37996

[4] Materials Science and Technology Division, Oak Ridge National Laboratory, Oak Ridge, TN 37831

[5] Departamento de Física - UFMG, Av. Antônio Carlos, 6627, Belo Horizonte, MG-Brazil 31270-901

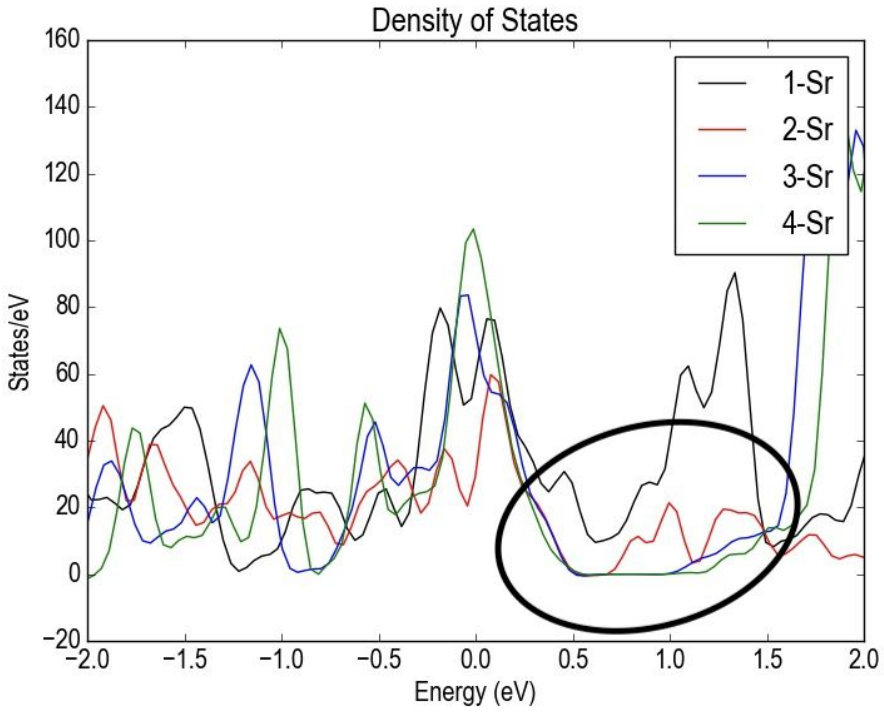

Figure S1: Density of states calculated via density functional theory. Density of states calculated for various Sr concentrations at the surface of $La_{(1-x)}Sr_xMnO_3$ (x=0.3) thin film. Black circle highlights band opening for increasing Sr surface coverage including 25% (black,1-Sr), 50% (red, 2-Sr), 75% (blue, 3-Sr), and 100% (green, 4-Sr).

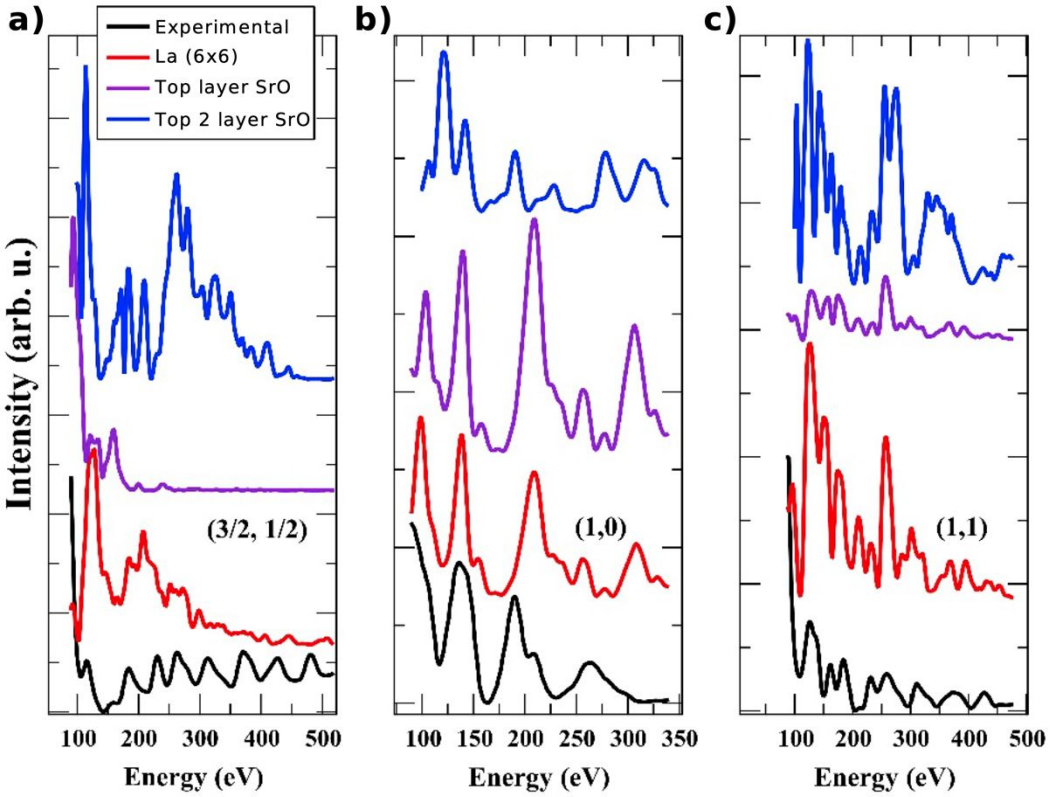

Figure S2: LEED (I-V) modeling. Models consist of a La (6x6) reconstruction (red), buckled single SrO top layer (purple), and two SrO top layers corresponding to a) (3/2,1/2), b) (1,0), and c) (1,1) LEED diffraction spots referenced in main text (Figure 1d). Note, black corresponds to experimental data.

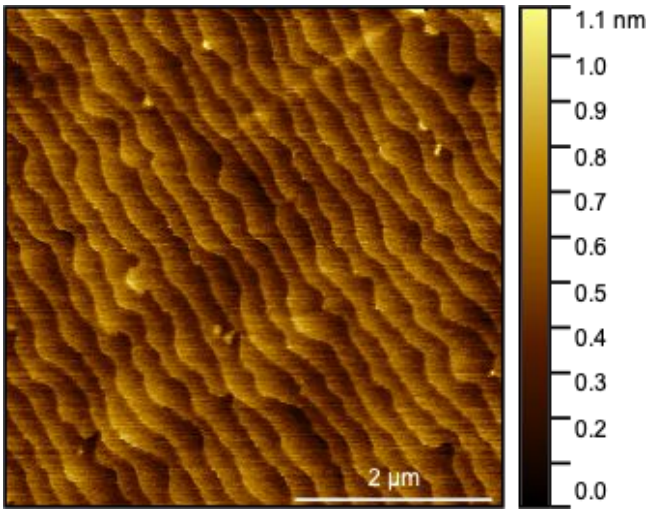

Figure S3: Atomic force microscope topography of $(001)_{pc}$ $NdGaO_3$ substrate representative of pre-growth template. Scale bar is 2µm.

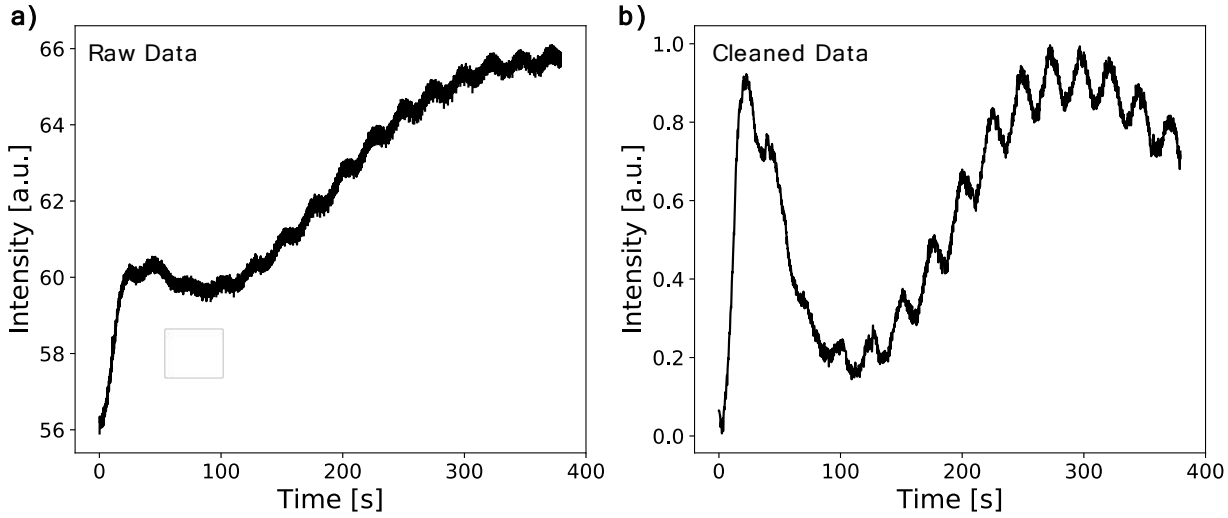

Figure S4: Reflection high energy electron diffraction profile with a) raw data, and b) normalized with background subtraction and Savitzky-Golay filter. Data shows approximately 15 oscillations. Note, profile was derived from an averaged 10x10 pixel area.

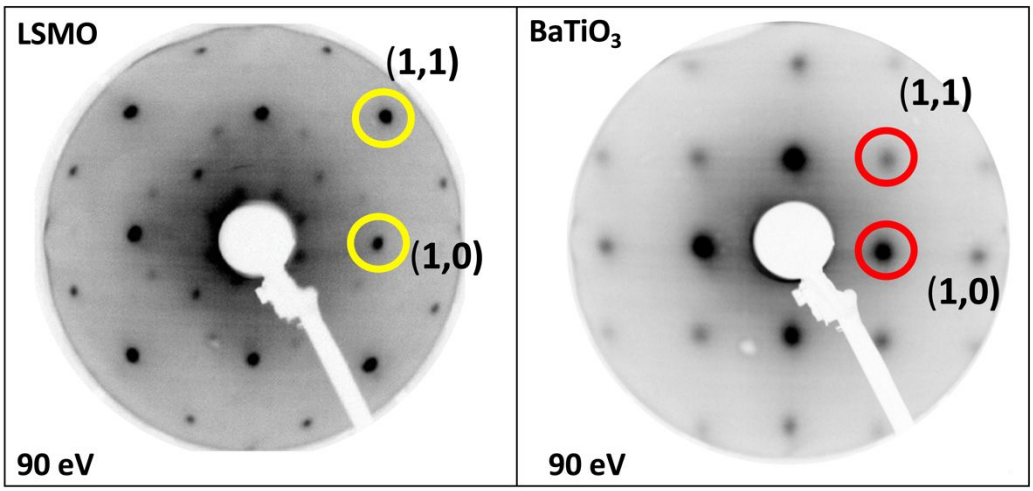

Figure S5: Experimental LEED patterns acquired at 90eV for LSMO (left) and $BaTiO_3$ (right) with identical LEED system and collection geometry. Yellow and red circles indicate (1,1) and (1,0) diffraction spots for LSMO and $BaTiO_3$, respectively.

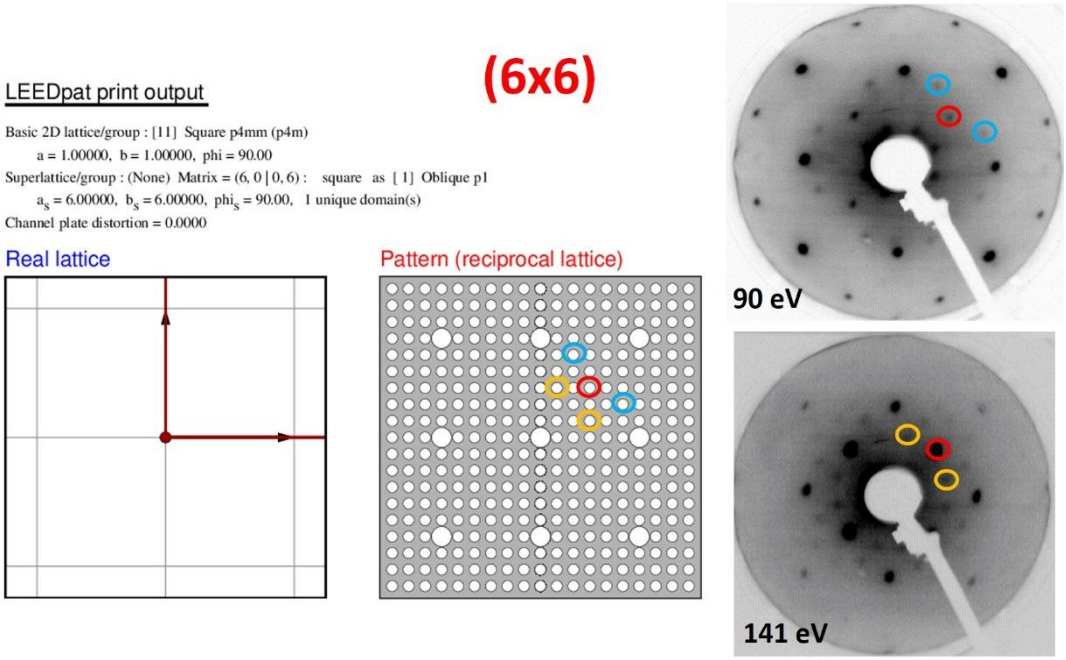

Figure S6: (6x6) LEEDpat simulated patterns comparison with actual LEED data collected at 90 and 141 eV for LSMO. In the simulated diffraction pattern the large and small white dots corresponds to integer and fractional spots respectively.

Element	Energy	Transmission at 40 eV pass Medium Area Slits 7x20mm Iris 20	Transmission Function x 1000	Normalized to O1s
La 3d	836	0.00717	7.17	0.950
La 4d	103	0.00664	6.64	0.880
Sr 3d	134	0.00674	6.74	0.893
Sr 3p	270	0.00720	7.20	0.954
Mn 3p	639	0.00768	7.68	1.017
O 1s	530	0.00755	7.55	1.000

Table S1: Analyzer transmission function values from PHOIBOS-150 hemispherical analyzer manufacture specific to pass energy, lens mode, slits, and iris used during data collection.

LEED I-V Analysis

In the LEED-IV analysis, we employed the use of the Pendry R-factor[1] and tested four structural models for our (6x6) reconstructed surface. It is important to note, no structural optimization was performed in this comparison since there is not enough experimental energy range to justify such procedure. The LEEDFIT code was employed to generate theoretical I-V curves and R-factor calculations for the following four models:

1. Model 1: substitutional La atom in top SrO layer;
2. Model 2: extra Sr atom on top of SrO layer;
3. Model 3: top MnO_2 layer;
4. Model 4: 2 SrO top layers;

The final Pendry R-Factor values obtained for the different structural models are presented here:

Model	Pendry R-factor with uncertainty[1]
1	**(0.94 ± 0.17)**
2	**----------**
3	**(0.86 ± 0.15)**
4	**(0.89 ± 0.16)**

Table S2: Pendry R-Factor values with uncertainty calculated for the four models.

Model 2 presented bad theory-experiment agreement for the fractional I-V curves, and thus problems in the R-factor calculation. These problems primarily originated from the very low intensities obtained for the theoretical fractional diffracted bean. Structural model 2 was consequently discarded.

By inspecting the final R-factor values obtained for models 1, 3 and 4, and considering their uncertainties, it is virtually impossible to point out a preferential candidate structure for the (6x6) structural reconstruction. However, model 3 (top MnO_2) layer can be discarded based on our XPS analysis. Our *ab initio* results also favor model 1 in contrast to model 4 as the possible structure for the (6x6) reconstruction. In summary, by combining qualitative LEED-IV analysis with other experimental and theoretical information, we have identified model 1 as the most possible candidate for the (6x6) reconstruction.

References

1. Pendry, J. B. Reliability factors for LEED calculations. *J. Phys. C Solid State Phys.* **13**, 937–944 (1980).